JCI insight

Reversal of ciliary mechanisms of disassembly rescues olfactory dysfunction in ciliopathies

Chao Xie, … , Robert J. Campbell, Jeffrey R. Martens

JCI Insight. 2022. https://doi.org/10.1172/jci.insight.158736.

Research In-Press Preview Cell biology Genetics

Graphical abstract

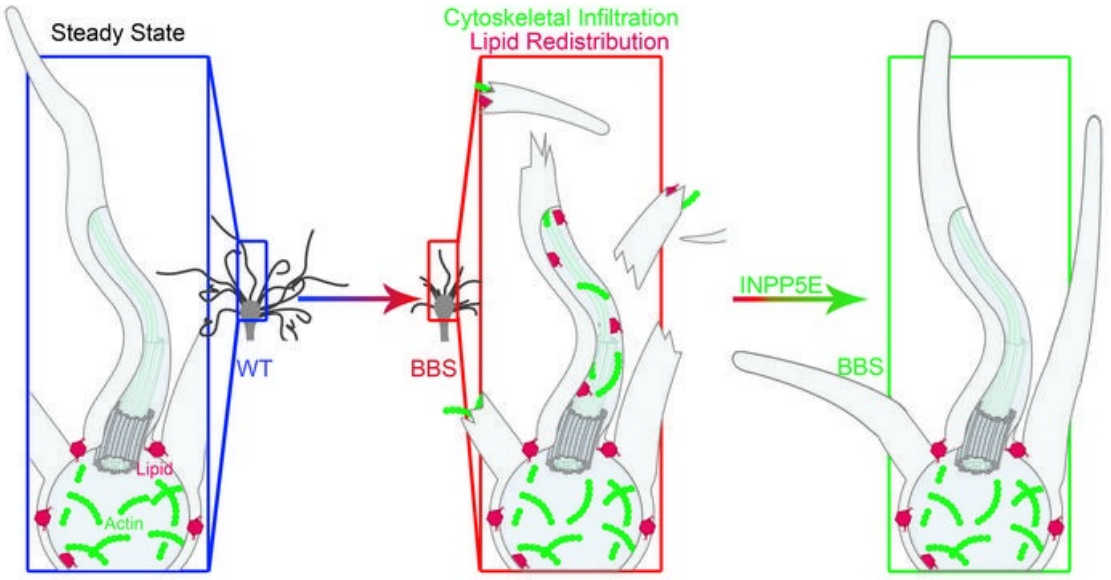

Reversal of ciliary mechanisms of disassembly rescues olfactory dysfunction in ciliopathies

Chao Xie[1,2], Julien C. Habif[1,2], Kirill Ukhanov[1,2], Cedric R. Uytingco[1,2], Lian Zhang[1,2], Robert J. Campbell[1,2], and Jeffrey R. Martens[1,2,3]

[1] Department of Pharmacology and Therapeutics, and [2] Center for Smell and Taste, University of Florida College of Medicine, Gainesville, FL 32610, USA.

[3]Corresponding author: Jeffery R. Martens, Department of Pharmacology and Therapeutics, University of Florida, 1200 Newell Drive, PO Box 100267, Gainesville, FL 32610-0267, USA. Telephone Number: (352)294-5352, E-mail: martensj@ufl.edu

Conflict-of-interest statement: The authors have declared that no conflict of interest exists.

Abstract.

Ciliopathies are a class of genetic diseases resulting in cilia dysfunction in multiple organ systems, including the olfactory system. Currently, there are no available curative treatments for olfactory dysfunction and other symptoms in ciliopathies. The loss or shortening of olfactory cilia, as seen in multiple mouse models of the ciliopathy Bardet-Biedl syndrome (BBS), results in olfactory dysfunction. However, the underlying mechanism of the olfactory cilia reduction is unknown, thus limiting the development of therapeutic approaches for BBS and other ciliopathies. Here, we demonstrated that $PI(4,5)P_2$, a phosphoinositide typically excluded from olfactory cilia, aberrantly redistributed into the residual cilia of BBS mouse models, which caused F-actin ciliary infiltration. Importantly, $PI(4,5)P_2$ and F-actin were necessary for olfactory cilia shortening. Using a gene therapeutic approach, the hydrolyzation of $PI(4,5)P_2$ by overexpression of INPP5E restored cilia length, and rescued odor detection and odor perception in BBS. Together, our data indicate that $PI(4,5)P_2$ and F-actin-dependent cilia disassembly is a common mechanism contributing to the loss of olfactory cilia in BBS and provide valuable pan therapeutic intervention targets for the treatment of ciliopathies.

Keywords: Cilia disassembly; gene therapy; ciliopathies; olfactory cilia.

Introduction.

Cilia are evolutionary conserved, microtubule-based organelles that are present on the surface of most cell types in vertebrates (1). The enrichment of various receptors and other ciliary exclusive proteins (2, 3) makes the cilium a unique organelle with critical roles in numerous developmental and fundamental physiological processes (4-6). Genetic defects of ciliary proteins that are necessary for cilia biogenesis, maintenance, and/or function, can result in a broad class of human diseases and developmental disorders, termed ciliopathies (7). As one class of ciliopathies, Bardet-Biedl syndrome (BBS) can manifest as a constellation of symptoms including obesity, renal dysfunction, male infertility, skeletal malformation, cognitive defects, and retinal degeneration (8-10). Furthermore, BBS has been characterized as a major genetic cause of olfactory dysfunction (9-11), which is a relatively common disorder (12) that markedly decreases the quality of life and increases the risk of injuries (13). Besides symptom management, there are no curative treatment options currently available for BBS and other ciliopathies. Several preclinical studies have shown that single gene replacement is a promising curative therapeutic approach for olfactory dysfunction in ciliopathies (9, 10, 14), however, it is only limited to the treatment of a small subset of patients with genetic mutations in the targeted gene (15).

BBS is caused by one or more mutation(s) in any of at least 21 proteins related to the BBSome, which is a highly conserved complex comprised of eight core BBS proteins including BBS1, BBS2, BBS4, BBS5, BBS7, BBS8, BBS9, and BBS18/BBIP10 (16, 17). The BBSome mainly functions as a cargo adaptor for intraflagellar transport (IFT) that regulates protein ciliary trafficking (16, 18, 19). The mutation or deletion of BBSome related genes typically alters morphology, length, and dynamics of cilia in different organ systems with diverse effects on cilium maintenance (9-11, 20). In the olfactory system, olfactory cilia extend from olfactory sensory neurons (OSNs) providing a large odorant receptive field (5, 21). Defects in olfactory cilia, as seen in animal models of BBS, lead to significant impairment(hyposmia) or complete loss (anosmia) of olfactory function (9, 10, 14, 22). Studies have shown that BBS mouse models share similar olfactory phenotypes,

specifically with decreased olfactory cilia length and number (9-11, 23, 24), suggesting that a shared mechanism may contribute to the pathogenesis of BBS. However, the detailed mechanism of olfactory cilia reduction in BBS has not been determined, the understanding of which may offer novel therapeutic targets for BBS.

In normal conditions, cilia are dynamic structures with a tightly regulated balance between cilia formation, maintenance, and disassembly (25, 26). Different ciliopathies can be caused by dysfunction in any of these three ciliary processes. In the context of BBS, olfactory cilia are reduced but not completely lost and the residual cilia still have a persistent trafficking of both IFT and protein, which is essential for cilia maintenance (9, 10). These indicate that olfactory cilia formation and maintenance may not be impacted in BBS. Importantly, there is a progressive loss of olfactory cilia resulting from the deletion of BBS4 (9). Together, these pieces of evidence suggest that olfactory cilia form and maintained properly but that olfactory cilia disassembly may contribute to the loss of cilia in BBS. A recent study in vitro in cultured cells shows that the normal process of primary cilia resorption that occurs during the cell cycle involves membrane composition remolding that contributes to primary cilia disassembly (27). The membrane composition in cilia is unique and different from that of the cellular membrane (28-31). For instance, $PI(4,5)P_2$ (Phosphatidylinositol 4,5-Bisphosphate), a phospholipid component of the cell membrane, is enriched at the base of cilia but is excluded from the ciliary membrane due to the presence of its hydrolase, INPP5E (Inositol Polyphosphate-5-Phosphatase E) (32-35). In culture, growth stimulation of quiescent cells results in the accumulation of $PI(4,5)P_2$ in primary cilia and promotes cilia disassembly (27). Importantly, BBS5 contains two lipid-binding Pleckstrin Homology (PH) like domains, which facilitates the direct interaction between the BBSome and phospholipids (16). Furthermore, BBS4 is implicated in regulating the ciliary distribution of INPP5E in primary cilia (36), suggesting that the BBSome plays important roles in the regulation of the ciliary membrane composition. However, all of these studies were conducted in cultured, dividing cells in primary cilia, which are remarkably different from olfactory cilia in the terminally

differentiated neurons (5, 21). It is largely unclear if such lipid remolding can take place in olfactory cilia in vivo or if it also contributes to the pathogenesis of BBS disease in the olfactory system. In the current study, we investigate the signaling mechanisms underlying the loss or shortening of olfactory cilia under pathological conditions in BBS mutant mice. Importantly, using a gene therapeutic approach, we demonstrate that olfactory dysfunction in BBS can be rescued by targeting a common factor that regulates the ciliary length. This mechanistic study highlights alternative therapeutic targets for treating ciliary dysfunction in ciliopathies, which in the future may allow gene therapy to move beyond single gene replacement.

Results.

$PI(4,5)P_2$ aberrantly redistributes into residual olfactory cilia in *Bbs4*^{KO} mice.

To understand the underlying mechanism of olfactory cilia shortening in BBS, and investigate if lipid remolding occurs in olfactory cilia in vivo, we examined the olfactory ciliary distribution of $PI(4,5)P_2$ in *Bbs4*^{KO} mouse model (9). Wildtype (WT) and *Bbs4*^{KO} mice were intra-nasally co-infected with myristoylated-palmitoylated-mCherry (MP-mCherry) and PLCδ1PH-GFP adenovirus (AV). MP-mCherry is an inert lipid-anchored fluorophore and was used to mark the full length of olfactory cilia [9,(18)]. The PLCδ1-PH domain binds to $PI(4,5)P_2$ with high affinity and therefore was applied to label the endogenous $PI(4,5)P_2$ (35). *En face* confocal imaging was performed 10 days post the virus infection (37). Previous work in the lab has shown that the mature OSNs are the only neurons in the OE that can be infected by adenovirus (38). As in the previous study(9), *Bbs4*^{KO} OSNs have significantly shorter and fewer olfactory cilia compared with WT OSNs **(Fig.1A&B** left panel **& Fig.1C)**. Interestingly, $PI(4,5)P_2$ olfactory ciliary distribution was significantly different between the WT and the *Bbs4*^{KO} groups (**Fig.1**). As shown in the representative images, the distribution of $PI(4,5)P_2$ was restricted to the knob of the majority OSNs in the WT mice (**Fig.1A**, middle panel). However, $PI(4,5)P_2$ lost its restriction in the knob of OSNs and aberrantly redistributed into the residual olfactory cilia in the *Bbs4*^{KO} mice (**Fig.1B**, middle

panel). The relative PI(4,5)P_2 positive cilia length to the full length of the cilia increased from 8.347 ±1.950 % in the WT group to 88.98 ± 2.078% in the *Bbs4*^{KO} group **(Fig.1D**, left**).** The percentage of PI(4,5)P_2 positive cilia number per OSN significantly changed from 8.399 ± 2.102% in the WT group to 94.63 ±1.649% in the *Bbs4*^{KO} group **(Fig.1D**, right**)**.

To further explore if PI(4,5)P_2 ciliary mislocalization is a shared mechanism underlying olfactory dysfunction in ciliopathies, we investigated the PI(4,5)P_2 ciliary distribution in different ciliopathies including *Bbs1*$^{M390R/M390R}$ and *Ift88*^{OSNKO} mouse models, which all have been shown to have shortened olfactory cilia (10, 14). Interestingly, similar to *Bbs4*^{KO}, the *Bbs1*$^{M390R/M390R}$ group had abnormal PI(4,5)P_2 ciliary localization **(Supplemental Fig.1C)**. However, this effect differed in *Ift88*^{OSNKO} olfactory cilia, in which much shorter and fewer cilia had PI(4,5)P_2 ciliary localization**(Supplemental Fig.1B&D&E).** Compared with the WT and *Ift88*^{OSNKO} mice, the percentage of PI(4,5)P_2 positive cilia number and the relative PI(4,5)P_2 positive cilia length were significantly increased in the *Bbs1*$^{M390R/M390R}$, and *Bbs4*^{KO} mice **(Supplemental Fig.1D&E)**. Together, these results show that PI(4,5)P_2 abnormally redistributes into the olfactory cilia in BBS mouse models, which indicates that PI(4,5)P_2 ciliary redistribution is a shared mechanism for olfactory cilia shortening in BBS mutant mice.

PI(4,5)P_2 is necessary for olfactory cilia shortening in *Bbs4*^{KO} mice.

Next, to determine if PI(4,5)P_2 ciliary redistribution is necessary for olfactory cilia shortening, *Bbs4*^{KO} mice were adenovirally infected with MP-iRFP and GFP-INPP5E **(Fig.2A)**, which specifically hydrolyzes PI(4,5)P_2 in cilia (35). A catalytically inactive isoform of INPP5E, GFP-INPP5E (D477N) (35), together with MP-iRFP, were administered to a different group of *Bbs4*^{KO} mice and served as the negative control group **(Fig.2B)**. The olfactory cilia length per OSN was measured 10 days post-viral infection. The *Bbs4*^{KO} mice receiving GFP-INPP5E (D477N) still maintained comparable olfactory cilia length per OSN to the untreated OSNs from the same animal **(Fig.2C)**. Intriguingly, ectopic treatment with wildtype INPP5E but not with INPP5E (D477N)

partially rescued olfactory cilia length in *Bbs4*^{KO} mice **(Fig.2)**. Importantly, our data demonstrate that membrane remodeling of PI(4,5)P_2 is necessary for olfactory cilia shortening in *Bbs4*^{KO} mice.

Overexpression of INPP5E rescues *Bbs4*^{KO} mice peripheral odor detection.

Defects in olfactory cilia have been shown to impair the peripheral odor detection in *Bbs4*^{KO} mice (9). To test whether the partial restoration of cilia length by INPP5E treatment was sufficient to restore peripheral odor detection, we performed electro-olfactogram (EOG) recording to measure the odor-evoked field potential responses on the surface of the olfactory epithelium (OE) (9, 10, 14). Compared with the untreated group, *Bbs4*^{KO} mice receiving GFP-INPP5E showed a significantly increased electrical response to different concentrations of amyl acetate (AA) including 10^{-5}M, 10^{-4} M, 10^{-2}M, and 10^{0}M, as well as to cineole (equal vapor pressure with 10^{-3}M AA and 10^{-2}M AA) (**Fig. 3A&B**). The GFP-INPP5E (D477N) treatment in *Bbs4*^{KO} mice did not change their peripheral odor detection **(Supplemental Fig.2)**. These data show that blocking of PI(4,5)P_2 ciliary distribution by INPP5E treatment can restore the cellular odor detection in populations of peripheral olfactory neurons of *Bbs4*^{KO} mice.

The *Bbs4*^{KO} mice have an impaired odor detection threshold, which can be rescued by the treatment of INPP5E.

To further examine the therapeutic potential of INPP5E treatment in the restoration of the olfactory function, we explored the odor perception/odor detection threshold of *Bbs4*^{KO} mice using whole-body plethysmography. This method takes advantage of a mouse's innate increase in sniffing rate upon detection of a novel odorant (39) and provides a sensitive behavioral platform to quantify odor perception. As shown in the representative trace of a sniffing response to 10^{-12} Torr (1 Torr = 133.32 Pa) of hexanal, the sniffing rate of the WT mouse immediately elevated following the odor delivery, indicating the detection of odor **(Fig.3C)**. However, the sniffing rate of the *Bbs4*^{KO} mouse did not change upon the odor delivery at the same vapor pressure, which demonstrated a

deficiency in odor perception in *Bbs4*^{KO} mice **(Fig.3C)**. Furthermore, our data showed that *Bbs4*^{KO} mice did not increase their sniffing rate until 10^{-6} Torr of odor delivery **(Supplemental Fig.3)**, indicating that *Bbs4*^{KO} is a hyposmic model rather than an anosmic model. In comparison with WT, *Bbs4*^{KO} mice showed significantly higher odor detection thresholds (low odor detection sensitivity). More importantly, GFP-INPP5E treated *Bbs4*^{KO} mice exhibited an increased sniffing rate following odor delivery of 10^{-12}Torr **(Fig.3C&D)**, and 10^{-10}Torr **(Fig.3D)**. All mice in different groups showed comparable sniffing response following 10^{-4}Torr odorants delivery **(Fig.3D)**. Together, these data show that INPP5E treatment increases olfactory cilia length to restore whole animal odor perception suggesting that ectopic overexpression of INPP5E is a potential treatment for olfactory dysfunction in BBS.

F-actin infiltrates into olfactory cilia in *Bbs4*^{KO} mice.

Next, we explored how membrane lipid remodeling induced olfactory cilia disassembly in BBS. PI(4,5)P_2 functions as an important regulator of actin cytoskeletal dynamics in cells (40, 41). Elevated levels of PI(4,5)P_2 regulate the activities of several F-actin regulatory proteins and therefore promotes the polymerization of F-actin in cells (41). Recently, PI(4,5)P_2 was shown to induce intraciliary polymerization of F-actin (27), which has emerged as a major player in the disassembly of primary cilia in vitro (15, 27, 42, 43). To understand if PI(4,5)P_2 olfactory ciliary remodeling induces F-actin ciliary infiltration, we measured F-actin olfactory ciliary localization in the *Bbs4*^{KO} mouse model. The WT and *Bbs4*^{kO} mice were intra-nasally co-infected with MP-mCherry and Lifeact7-GFP adenovirus to label the full length of olfactory cilia and the endogenous F-actin, respectively (9, 44). Interestingly, our data revealed that F-actin olfactory ciliary distribution was significantly different between the WT and the *Bbs4*^{KO} groups (**Fig.4A-D**). For the majority of OSNs in the WT group, F-actin localized in the knob of OSNs and was excluded from the olfactory cilia (**Fig.4A**). This was consistent with the current understanding that F-actin is excluded from the cilia structure (45). However, F-actin lost its restriction in the knob of OSNs and

aberrantly infiltrated into olfactory cilia in *Bbs4*^{KO} mice (**Fig.4B**). The analysis of the data showed that the percentage of F-actin positive cilia number per OSN significantly increased from 10.37±1.615% in the WT group to 77.32 ± 2.494% in the *Bbs4*^{KO} group (**Fig.4C**). The relative F-actin positive cilia length to the full length of the cilia significantly elevated from 1.751± 0.3133% in the WT group to 66.31± 2.531% in the *Bbs4*^{KO} group (**Fig.4D**).

To compare the F-actin ciliary localization in different ciliopathy mouse models with shortened olfactory cilia we investigated its distribution in both *IFT88*^{OSNKO}, and *Bbs1*$^{M390R/M390R}$ (10, 14) . Similar to PI(4,5)P_2, F-actin did not show abundant ciliary redistribution in *Ift88*^{OSNKO} olfactory cilia **(Supplemental Fig.4B)**, but F-actin aberrantly infiltrated into *Bbs1*$^{M390R/M390R}$ olfactory cilia **(Supplemental Fig.4C)**. Compared with the WT and *Ift88*^{OSNKO} mice, the percentage of F-actin positive cilia number and the relative F-actin positive cilia length were significantly increased in the *Bbs1*$^{M390R/M390R}$ mice **(Supplemental Fig.4D&E)**. Together, these results show that F-actin abnormally infiltrates into the olfactory cilia in BBS mouse models but not in at least one other ciliopathy mouse model, indicating that the ciliary redistribution of F-actin is a shared mechanism for olfactory cilia shortening in BBS mutant mice.

F-actin is necessary for olfactory cilia shortening in *Bbs4*^{KO} mice.

We further evaluated the necessity of F-actin ciliary redistribution for olfactory cilia shortening in *Bbs4*^{KO} by targeted overexpression of Thymosin-β4 (Tβ4), which sequesters G-actin from incorporation into actin filaments and therefore regulates actin polymerization (46). Tβ4 was fused to a ciliary localized GPCR, 5HT6, which efficiently targeted Tβ4 into olfactory cilia to specifically suppress intraciliary F-actin **(Supplemental Fig.5)** (27). The *Bbs4*^{KO} mice were divided into two groups and infected with either adenovirus containing 5HT6-YFP-Tβ4 or 5HT6-YFP-Tβ4 (K18E/K19E). The 5HT6-YFP-Tβ4 (K18E/K19E) is an actin-binding deficient mutant (27) and therefore serves as the negative control. As expected, the adenoviral treatment with the 5HT6-YFP-Tβ4 (K18E/K19E) did not affect olfactory cilia length in *Bbs4*^{KO} mice (**Fig. 4F**), which still

have comparable olfactory cilia length per OSN to the untreated OSNs from *Bbs4*^{KO} mice **(Fig.2C)**. Importantly, the expression of 5HT6-YFP-Tβ4 in *Bbs4*^{KO} significantly increased the olfactory cilia length per OSN(**Fig. 4E&F**), which was relatively shorter than that in WT group **(Fig.2C)**, suggesting that 5HT6-YFP-Tβ4 partially rescued *Bbs4*^{KO} olfactory cilia length. These data show that F-actin ciliary redistribution is necessary for olfactory cilia shortening *in Bbs4*^{KO} mice.

PI(4,5)P_2 regulates F-actin olfactory ciliary distribution in *Bbs4*^{KO} mice.

To understand if PI(4,5)P_2 is involved in the regulation of actin polymerization in olfactory cilia, we investigated the interrelationship between PI(4,5)P_2 and F-actin in olfactory cilia. Excitingly, our data showed that F-actin exclusion from cilia was re-established by blocking PI(4,5)P_2 ciliary redistribution in GFP-INPP5E treated *Bbs4*^{KO} mice **(Fig.5A)**. As expected, F-actin still redistributed into the olfactory cilia in the GFP-INPP5E (D477N) treated *Bbs4*^{KO} group **(Fig.5B)**, in which PI(4,5)P_2 localized to cilia. On the contrary, blocking ciliary F-actin by 5HT6-YFP-Tβ4 failed to prevent PI(4,5)P_2 ciliary redistribution in *Bbs4*^{KO} mice **(Fig.5C)**. Together, these results show that ciliary localized PI(4,5)P_2 directly regulates F-actin olfactory ciliary redistribution in *Bbs4*^{KO} mice.

***Bbs4* single gene replacement restores olfactory ciliary exclusion of F-actin and PI(4,5)P_2 in *Bbs4*^{KO} mice.**

It has been demonstrated that intranasal adenoviral and adeno-associated viruses (AAV) mediated gene delivery of wild-type genes are capable of restoring ciliary morphology and olfactory function in ciliopathy mouse models (9, 10, 14). The olfactory cilia shortening in *Bbs4*^{KO} can be partially rescued by *Bbs4* gene replacement (9). To investigate the underlying mechanism of this ciliary length rescue, we explored the ciliary distribution of F-actin and PI(4,5)P_2 following *Bbs4* single gene replacement. Compared with the untreated group, OSNs in *Bbs4*^{KO} mice with the expression of BBS4-mCherry showed no F-actin ciliary localization **(Supplemental Fig.6A)**.

Furthermore, normal ciliary distribution of PI(4,5)P_2 in OSNs was restored in *Bbs4*^{KO} mice after *Bbs4* gene replacement **(Supplemental Fig.6B)**. Overall, these data suggest that *Bbs4* gene replacement rescues olfactory cilia length in *Bbs4*^{KO} mice by excluding abnormally distributed F-actin and PI(4,5)P_2 in olfactory cilia.

Discussion.

Our work demonstrates for the first time that aberrant ciliary redistribution of PI(4,5)P_2 and F-actin are necessary for olfactory cilia disassembly and contribute to the pathogenesis of BBS **(Fig.6)**. More importantly, blocking PI(4,5)P_2 and F-actin ciliary mislocalization by adenoviral expression of INPP5E restores olfactory cilia length in *Bbs4*^{KO} mice **(Fig.6)**, which is sufficient to rescue peripheral odor detection and re-establish odor perception at the whole animal level. This study provides valuable novel insights into mechanisms of olfactory cilia disassembly in pathological conditions and highlights viable candidate targets for the treatment of olfactory dysfunction and other symptoms of ciliopathies.

Olfactory cilia have unique membrane lipid compositions (35) due to the presence of the transition zone (TZ), which strictly controls the localization of ciliary protein and membrane lipids(32, 47-49). Ciliary phosphoinositides are emerging as critical regulators in primary cilia (50), however, their role in the biogenesis and maintenance of olfactory cilia are poorly understood. PI(4,5)P_2 is a phosphoinositide that is restricted to the membrane of the ciliary base and is absent from cilia as a result of its hydrolyzation by INPP5E(27, 32-35). Intriguingly, our in vivo work revealed for the first time that not only is PI(4,5)P_2 aberrantly redistributed into cilia in terminally differentiated neurons of BBS mice **(Fig.1&Supplemental Fig.1)**, but that it is necessary for olfactory cilia shortening **(Fig.2)**. This finding is supported by studies of primary cilia, where the ciliary remodeling of PI(4,5)P_2 caused cilia disassembly or ciliary fission in cells entering the cell cycle, as well as those under normal and agonist stimulation conditions (27, 51). Although different in that cell cycle mediated cilia disassembly is a normal physiological process, our study in non-

dividing neurons in pathological conditions shows a similar mechanism involved in the loss of cilia. This suggests that the aberrant ciliary redistribution of $PI(4,5)P_2$ is a conserved mechanism involved in the disassembly of cilia. Additionally, there is controversy regarding the sufficiency of $PI(4,5)P_2$ ciliary redistribution for cilia shortening, as its accumulation had opposing effects on the primary cilia of two distinct cell types(27, 49, 51). Interestingly, our previous study showed that $PI(4,5)P_2$ ciliary redistribution through deletion of INPP5E in OSNs did not reduce olfactory ciliary length (35). Together, our studies suggest that the ciliary mislocalization of $PI(4,5)P_2$ is necessary but not sufficient for olfactory cilia shortening and highlight that the role of $PI(4,5)P_2$ in the maintenance of cilia is cell type specific.

In addition to $PI(4,5)P_2$, the role of other ciliary phosphoinositides in olfactory cilia is largely underexplored. For instance, our previous work showed that PI(3,4,5)P3 (phosphatidylinositol-3,4,5-trisphosphate) was restricted mostly to the knobs of OSNs with relatively low presence in olfactory cilia (35). Depletion of PTEN (Phosphatase and tensin homologue), an enzyme converting PI(3,4,5)P3 to $PI(4,5)P_2$ (52), promoted primary cilia disassembly(53), suggesting that PI(3,4,5)P3 may be involved in the process of cilia disassembly. Further efforts should be made to explore the role of other ciliary phosphoinositides in regulating the dynamics of olfactory cilia.

As microtubule-based organelles, olfactory cilia, like other types of cilia, were believed to not contain F-actin. However, emerging work in cultured cells has shown that primary cilia disassembly can occur through F-actin–dependent mechanisms in both agonist and growth stimulation conditions (26, 27, 42). Excitingly, our observations showed that in BBS F-actin abnormally infiltrated into olfactory cilia **(Fig.4A-D)**. Importantly, overexpression of the actin-sequestering protein Thymosin β4 (Tβ4) significantly rescued olfactory cilia length in BBS **(Fig.4E&F)**, providing strong evidence that the loss of olfactory cilia in BBS is mediated by F-actin-dependent cilia disassembly. This raises a question of whether F-actin-dependent cilia disassembly is a conserved mechanism for cilia loss in other ciliopathies. Interestingly, the

299 treatment of Cytochalasin D has been implicated in restoring the loss of primary cilia in cultured
300 cells with the IFT88 hypomorphic mutation (orpk/orpk) (54), suggesting that F-actin contributed to
301 the loss of primary cilia in the IFT88 mutant model. In contrast, our results showed that F-actin
302 displayed a different olfactory ciliary distribution pattern in *Ift88*^{OSNKO} than in BBS **(Supplemental**
303 **Fig.4B&D&E)**. The seemingly contradictory findings may be explained by differences between
304 cilia types and working models. Nevertheless, our work suggests that the loss of olfactory cilia in
305 *Ift88*^{OSNKO} is not caused by F-actin mediated cilia disassembly, but likely induced by dysfunction
306 of cilia assembly due to the disruption of IFT. Regardless, F-actin emerges as a candidate target
307 in the treatment of olfactory cilia dysfunction induced by cilia disassembly.
308 An important question to understand the mechanisms of olfactory cilia disassembly, is the timing
309 of each step. Our results proved that the ciliary infiltration of F-actin was induced by the ciliary
310 redistribution of PI(4,5)P_2 **(Fig.5)**, and is supported by results in primary cilia (27, 51). This
311 provides further insight into how membrane remolding induces olfactory cilia disassembly in BBS.
312 Within cells, PI(4,5)P_2 is an important regulator of actin dynamics through interactions with actin
313 regulatory proteins(55). In fact, in vitro studies show that the loss of actin regulators that facilitate
314 the polymerization of actin significantly increased primary cilia length(54, 56, 57),. This indicates
315 that actin regulators may be highly involved in the shortening of olfactory cilia in BBS. Therefore,
316 additional work is necessary to understand which and how actin regulators may participate in
317 olfactory cilia shortening in BBS.
318 BBS is a highly pleiotropic disease associated with variable penetrance and phenotypes within
319 different organ systems (8, 58). The deletion or mutation of BBS proteins markedly decreases
320 cilia length and number in OSNs (9, 10) but not in several other ciliated systems including the
321 brain(20, 59), the respiratory system (9, 24, 60), and kidney cells (61), suggesting that the
322 BBSome functions in the maintenance of olfactory cilia may be unique (9, 21). The results that
323 PI(4,5)P_2 and/or F-actin abnormally localize to olfactory cilia in multiple BBS, but not in *Ift88*^{OSNKO}
324 **(Supplemental Fig.1&Supplemental Fig.4)**, may reveal a novel role of the BBSome in OSNs.

The ectopic expression of WT BBS4 prevented PI(4,5)P_2 and F-actin ciliary mislocalization, suggesting that the BBSome may be required for the proper ciliary localization of phospholipid and actin filaments. These concepts are supported by evidence from other cilia types (62, 63) (16). Our work provides direct evidence that the BBSome plays a significant role in regulating the integrity of olfactory cilia including the control of membrane lipid composition, which is critical for the maintenance of proper cilia length and function.

There are several intriguing yet unanswered questions, one of which is how PI(4,5)P_2 and F-actin aberrantly redistribute into olfactory cilia in BBS. Clues for potential underlying mechanisms may reside in studies in other cilia types. Evidence from zebrafish (64) and mice (36, 48) showed that the BBSome interacted with the TZ and had overlapping roles in regulating primary ciliogenesis (65). A study in human renal tubular cells showed that INPP5E was absent from primary cilia with a dysfunctional TZ (66). Importantly, deletion of BBS4 in mouse embryonic fibroblasts also resulted in a significantly reduced ciliary localization of INPP5E (36). Together, these pieces of evidence highlights a possible underlying mechanism whereby, dysfunction of the BBSome causes defects in the TZ, in turn decreasing the level of INPP5E thus inducing the ciliary accumulation of PI(4,5)P_2 and F-actin. Another question is, how PI(4,5)P_2 and/or F-actin ciliary mislocalization leads to shorter olfactory cilia. A potential mechanism is that the aberrant ciliary infiltration of F-actin disrupts the stability of the ciliary microtubule structure and causes cilia disassembly. Supporting evidence for this hypothesis is presented in a study of *Xenopus* egg extracts showing that branched F-actin generated a mechanical force that blocked microtubule growth and triggered the disassembly of microtubule structures (67). Alternatively, membrane tension plays crucial roles in regulating the dynamics of membrane and cellular processes. Studies have shown that a high concentration of PI(4,5)P_2 or F-actin in cells can result in an increase in membrane tension (68-70). Failure to maintain normal membrane tension can lead to membrane lysis (68, 70). Based on these finding, we hypithesize that ciliary mislocalized PI(4,5)P_2 and F-actin alter the ciliary membrane tension and impairs the dynamic of the ciliary membrane,

which in turn results in cilia shortening. These potential mechanisms describing the pathogenesis of BBS need to be examined in further studies.

Previous work in the lab demonstrated that the loss of BBS4 in mice causes defects in peripheral odor detection, by measure of EOG recordings(9). However, it remained unknown if loss of BBS4 induced odor perception defects at the whole animal level. Our work using whole-body plethysmography for the first time showed that *Bbs4*^{KO} mice had a higher odor detection threshold, meaning lower odor detection sensitivity, compared with WT mice. Importantly, *Bbs4*^{KO} mice showed a similar response to that of WT mice, following odor delivery of 10−6 Torr and higher vapor pressures. This result shows that *Bbs4*^{KO} mice have a shift in odor detection threshold instead of a complete loss of odor detection due to the shortened and loss of olfactory cilia. Our work proves that the *Bbs4*^{KO} mouse model is a hyposmic model rather than an anosmic model, which is consistent with clinical findings of BBS patients (24). The sniffing curves of *Bbs4*^{KO} and WT mice being similar at higher concentrations suggests that suprathreshold magnitude is unchanged in the *Bbs4*^{KO} mice. This highlights the tremendous spare capacity of the olfactory system, which likely helps to maintain the integrity of the neural circuitry necessary for odor perception. Furthermore, the partial recovery of olfactory cilia length by the overexpression of INPP5E in *Bbs4*^{KO} mice rescues the odor detection threshold, suggesting the restoration of olfactory input is necessary for the treatment of olfactory dysfunction. Together, these observations demonstrate the potential that olfactory dysfunction could be fully rescued in BBS patients.

Our work highlights the potential of utilizing common mechanisms in olfactory cilia shortening as therapeutic targets for the treatment of olfactory dysfunction in BBS and other ciliopathies. Gene therapy is a promising curative therapeutic approach for olfactory dysfunction in ciliopathies (9, 10, 14, 15). Single gene replacement mediated by intranasal adenoviral and/ or adeno-associated viruses (AAV) was capable of rescuing the morphology and odor detection of olfactory cilia in ciliopathy mouse models (9, 10, 14). However, the single gene replacement approach is limited

as it only can be applied to a subset of patients with dysfunction in the corresponding gene (15). Rather than using WT BBS4 gene replacement to rescue *Bbs4*^{KO} olfactory cilia, this study restored the cilia length by reversing the aberrant distribution of PI(4,5)P_2 and F-actin, two common factors that contribute to the pathogenesis of multiple BBS **(Fig.2&Fig.4E&F)**. Strikingly, the recovery of olfactory cilia length by INPP5E treatment was sufficient to restore peripheral odor detection and even rescue the odor perception in *Bbs4*^{KO} mice **(Fig.3)**, suggesting that INPP5E is a potential treatment for olfactory dysfunction in BBS. Beyond olfactory impairment, BBS is highly pleiotropic and thus future studies should investigate if a similar mechanism causes cilia disassembly and if INPP5E treatment could restore the morphology and function of cilia in other ciliated organ systems. Furthermore, it is possible that PI(4,5)P_2 and F-actin mediated cilia disassembly is not only involved in BBS cilia loss but also contributes to the pathogenesis of other ciliopathies. Overall, our work highlights the potential of INPP5E as a pan treatment for ciliopathies thus moving beyond single gene replacement and benefitting a broader patient population.

Methods.

Mice. The male and female mice were bred and maintained at the University of Florida. The *Bbs4*^{KO}, *Bbs1*$^{M390R/M390R}$, *IFT88*^{OSNKO} mice, and their wildtype (WT) littermates of both sexes were used for experiments. Genotyping was performed according to previously published work (9, 14, 20).

Plasmids and adenovirus production. Adenovirus MP-GFP, MP-mCherry, MP-iRFP, BBS4-mCherry, PLCδ1-PH–GFP, GFP-INPP5E, and GFP-INPP5E-D477N were validated and described previously (9, 10, 35). Plasmids containing cDNA fragments were provided as follows: Lifeact7-GFP: Addgene plasmid # 54610, deposited by Michael Davidson. 5HT6-YFP-Thymosin β4: Addgene plasmid # 96806; 5HT6-YFP-Thymosin β4(KK18,19EE) mutant: Addgene plasmid # 96807, all deposited by Takanari Inoue (27). As previously described (9), all cDNAs were fused with fluorescence expression sequence and inserted into the pAd/CMV/V5-DEST expression vector using Gateway technology (Invitrogen, Waltham, MA, USA). Adenovirus was produced and amplified in HEK293T cell using the ViraPower protocol (Invitrogen, Waltham, MA, USA). The Virapur Adenovirus mini purification Virakit (Virapur, San Diego, CA, USA) was used for the isolation and purification of adenovirus. The dialyzation of the virus was performed in 2.5% glycerol, 25 mM NaCl, and 20 mM Tris-HCl (pH 8.0) using a 10,000 MWCO Slide-A-Lyzer dialysis cassette (Thermo Fisher Scientific, Waltham, MA, USA) at 4°C overnight. Then adenovirus was aliquoted and stored at −80°C for experimentation.

Intranasal viral administration. Adenovirus coding for fluorescent-tagged target proteins was intra-nasally administered to mice at P7, P21, or 3-4 months of age, as previously described (9). To better perform the viral infection, mice at P7 and P21 were restricted by hand, and mice at 3-4 months were anesthetized with Ketamine/Xylazine. Using a pulled 1-mL syringe, the virus was administered by applying a series of small drops to the nasal cavity of mice. The intranasal

delivery of the virus takes turns between the right and left nostrils to avoid potential drowning. 10 days after the 3 subsequent days of the viral infection, the mice were used for experiments.

Live *en face* confocal imaging. The adenovirus infected animals (at the age of P21) were euthanized with CO_2 and then the olfactory turbinates were exposed as previous described(9). The tissue was placed with the turbinates surface facing down in a bath of freshly oxygenated artificial cerebrospinal fluid (ACSF) (124 mM NaCl, 3 mM KCL, 1 mM $MgCl_2$, 2 mM $CaCl_2$, 1.25 mM NaH_2PO_4, 26 mM $NaHCO_3$, 25 mM glucose) and was gently held down using a mesh within the chamber. The imaging was performed on a Nikon TiE-PFS-A1R confocal microscope (Nikon, Minato City, Tokyo, Japan). The images and cilia length measurements were processed and performed using Fiji-Image J. Final figures were assembled using Photoshop 6CS (Adobe, San Jose, CA, USA).

Electro-olfactogram Recording (EOG). After euthanizing with CO_2, the olfactory turbinates of mice (at the age of P30-P35) were exposed for EOG, which was recorded from multiple turbinates using a MultiClamp 700A amplifier controlled by pClamp software (Molecular Devices, San Jose, CA, USA). Electrodes were made from standard glass micropipettes filled with 0.5% SeaPlaque agarose (Sigma-Aldrich, St. Louis, MO, USA) in 1X PBS. All odorants, including amyl acetate (AA) and cineole (Sigma-Aldrich, St. Louis, MO, USA), were diluted in DMSO (Sigma-Aldrich, St. Louis, MO, USA) and mixed to the final working concentration (as shown in the figure) in ultrapure water. Then odorants were delivered in vapor-phase along with the humidified airflow to the surface of the tissue. Tissues were allowed 1 min between subsequent odor deliveries to reduce the adaptation of the EOG response to the previous odorant. The data were analyzed with Clampfit (Molecular Devices, San Jose, CA, USA).

Whole-body plethysmography. To avoid the potential artifact induced by the motivation deficits in global ciliopathy mouse models, whole-body plethysmography was employed to determine odor detection thresholds. The assay takes advantage of the innate behavior that mice have of

increasing their sniffing rate when presented with a novel stimulus(39, 71) . The whole-body plethysmography was controlled by the pClamp software (Molecular Devices, San Jose, CA). Mice at 3-4 months old were used for this test. Four odorants including hexanal, cineole, propionic acid, and amyl acetate (AA) (Sigma-Aldrich, St. Louis, MO, USA) were used in the experiment. All odorants were diluted in mineral oil (Sigma-Aldrich, St. Louis, MO, USA) in log series and delivered in the vapor-phase with constant air delivery (1L/min) into the plethysmograph chamber. To avoid the potential artifact induced by the background odor, the chamber, and the possible pressure changes which may be associated with the odor delivery, animals were habituated to the experimental setting, 20min/day with 10 times mineral oil vapor delivery within the chamber, for three days prior the experiment. The recordings were done on 4 consecutive days, each of which contained 10 trials of mineral oil followed by the delivery of an odorant at 10^{-12}, 10^{-10}, 10^{-8}, 10^{-7}, 10^{-6}, 10^{-5}, 10^{-4}, 10^{-3}, 10^{-2} and 10^{-1} Torr. The odor detection threshold data were collected from the response of each mouse to 4 different odorants. Sniffing frequency ratios (sniffing rate 5 seconds pre vs 5 seconds after odor delivery) was calculated with Clampfit (Molecular Devices, San Jose, CA, USA) and compared between groups.

Statistics. All values in results were presented as mean ± SEM. The graph making and statistical analysis were performed by GraphPad Prism 8 software (GraphPad, San Diego, CA, USA). The student's t-test (Two-tailed) was used for comparison of the results between two groups and one-way ANOVA was used to calculate the statistical significance among multiple groups. A P value less than 0.05 was considered significant. *, **, *** and **** indicates $p < 0.05$, $p < 0.01$, $p < 0.001$, and $p < 0.0001$ statistical differences between groups, respectively.

Study approval. All procedures involving animals in this study were approved by the University of Florida Institutional Animal Care and Use Committee (IACUC).

Author Contributions: C. Xie, and J. R. Martens designed the research experiments. C. Xie, J. C. Habif, and K. Ukhanov performed the experiments. C. Xie, K. Ukhanov, C. R. Uytingco, and L. Zhang generated reagents. C. Xie generated the figures and analyzed the data. C. Xie, and J. R. Martens wrote the manuscript, with J. C. Habif providing critical input. All authors participated in revising the final manuscript and approved the final version.

Acknowledgments.

The authors would like to thank Eszter Boldog for her artistic contribution to the cilia disassembly schematic. This work was supported by the National Institute of Deafness and Other Communication Disorders R01DC019345 (to Jeffrey. R. Martens).

References.

1. Zimmerman K, and Yoder BK. SnapShot: Sensing and Signaling by Cilia. *Cell.* 2015;161(3):692-.e1.
2. Mombaerts P. Molecular biology of odorant receptors in vertebrates. *Annu Rev Neurosci.* 1999;22:487-509.
3. Tuteja N. Signaling through G protein coupled receptors. *Plant Signal Behav.* 2009;4(10):942-7.
4. Bisgrove BW, and Yost HJ. The roles of cilia in developmental disorders and disease. *Development.* 2006;133(21):4131-43.
5. Jenkins PM, McEwen DP, and Martens JR. Olfactory cilia: linking sensory cilia function and human disease. *Chem Senses.* 2009;34(5):451-64.
6. Falk N, Lösl M, Schröder N, and Gießl A. Specialized Cilia in Mammalian Sensory Systems. *Cells.* 2015;4(3):500-19.
7. Oh EC, and Katsanis N. Cilia in vertebrate development and disease. *Development.* 2012;139(3):443-8.
8. Khan SA, Muhammad N, Khan MA, Kamal A, Rehman ZU, and Khan S. Genetics of human Bardet-Biedl syndrome, an updates. *Clin Genet.* 2016;90(1):3-15.
9. Uytingco CR, Williams CL, Xie C, Shively DT, Green WW, Ukhanov K, et al. BBS4 is required for intraflagellar transport coordination and basal body number in mammalian olfactory cilia. *J Cell Sci.* 2019;132(5).
10. Williams CL, Uytingco CR, Green WW, McIntyre JC, Ukhanov K, Zimmerman AD, et al. Gene Therapeutic Reversal of Peripheral Olfactory Impairment in Bardet-Biedl Syndrome. *Mol Ther.* 2017;25(4):904-16.
11. Tadenev AL, Kulaga HM, May-Simera HL, Kelley MW, Katsanis N, and Reed RR. Loss of Bardet-Biedl syndrome protein-8 (BBS8) perturbs olfactory function, protein localization, and axon targeting. *Proc Natl Acad Sci U S A.* 2011;108(25):10320-5.
12. Hüttenbrink KB, Hummel T, Berg D, Gasser T, and Hähner A. Olfactory dysfunction: common in later life and early warning of neurodegenerative disease. *Dtsch Arztebl Int.* 2013;110(1-2):1-7, e1.
13. Mobley AS, Rodriguez-Gil DJ, Imamura F, and Greer CA. Aging in the olfactory system. *Trends Neurosci.* 2014;37(2):77-84.
14. Green WW, Uytingco CR, Ukhanov K, Kolb Z, Moretta J, McIntyre JC, et al. Peripheral Gene Therapeutic Rescue of an Olfactory Ciliopathy Restores Sensory Input, Axonal Pathfinding, and Odor-Guided Behavior. *J Neurosci.* 2018;38(34):7462-75.
15. Xie C, and Martens JR. Potential therapeutic targets for olfactory dysfunction in ciliopathies beyond single gene replacement. *Chem Senses.* 2021.
16. Nachury MV, Loktev AV, Zhang Q, Westlake CJ, Peränen J, Merdes A, et al. A core complex of BBS proteins cooperates with the GTPase Rab8 to promote ciliary membrane biogenesis. *Cell.* 2007;129(6):1201-13.
17. Loktev AV, Zhang Q, Beck JS, Searby CC, Scheetz TE, Bazan JF, et al. A BBSome subunit links ciliogenesis, microtubule stability, and acetylation. *Dev Cell.* 2008;15(6):854-65.
18. Williams CL, McIntyre JC, Norris SR, Jenkins PM, Zhang L, Pei Q, et al. Direct evidence for BBSome-associated intraflagellar transport reveals distinct properties of native mammalian cilia. *Nat Commun.* 2014;5:5813.
19. Wingfield JL, Lechtreck KF, and Lorentzen E. Trafficking of ciliary membrane proteins by the intraflagellar transport/BBSome machinery. *Essays Biochem.* 2018.
20. Davis RE, Swiderski RE, Rahmouni K, Nishimura DY, Mullins RF, Agassandian K, et al. A knockin mouse model of the Bardet-Biedl syndrome 1 M390R mutation has cilia defects, ventriculomegaly, retinopathy, and obesity. *Proc Natl Acad Sci U S A.* 2007;104(49):19422-7.

21. McClintock TS, Khan N, Xie C, and Martens JR. Maturation of the Olfactory Sensory Neuron and Its Cilia. *Chem Senses.* 2020;45(9):805-22.
22. Hoffman HJ, Ishii EK, and MacTurk RH. Age-related changes in the prevalence of smell/taste problems among the United States adult population. Results of the 1994 disability supplement to the National Health Interview Survey (NHIS). *Ann N Y Acad Sci.* 1998;855:716-22.
23. Xie C, Habif JC, Uytingco CR, Ukhanov K, Zhang L, de Celis C, et al. Gene therapy rescues olfactory perception in a clinically relevant ciliopathy model of Bardet-Biedl syndrome. *FASEB J.* 2021;35(9):e21766.
24. Kulaga HM, Leitch CC, Eichers ER, Badano JL, Lesemann A, Hoskins BE, et al. Loss of BBS proteins causes anosmia in humans and defects in olfactory cilia structure and function in the mouse. *Nat Genet.* 2004;36(9):994-8.
25. Sánchez I, and Dynlacht BD. Cilium assembly and disassembly. *Nat Cell Biol.* 2016;18(7):711-7.
26. Mirvis M, Stearns T, and James Nelson W. Cilium structure, assembly, and disassembly regulated by the cytoskeleton. *Biochem J.* 2018;475(14):2329-53.
27. Phua SC, Chiba S, Suzuki M, Su E, Roberson EC, Pusapati GV, et al. Dynamic Remodeling of Membrane Composition Drives Cell Cycle through Primary Cilia Excision. *Cell.* 2017;168(1-2):264-79.e15.
28. Garcia-Gonzalo FR, Corbit KC, Sirerol-Piquer MS, Ramaswami G, Otto EA, Noriega TR, et al. A transition zone complex regulates mammalian ciliogenesis and ciliary membrane composition. *Nat Genet.* 2011;43(8):776-84.
29. Chih B, Liu P, Chinn Y, Chalouni C, Komuves LG, Hass PE, et al. A ciliopathy complex at the transition zone protects the cilia as a privileged membrane domain. *Nat Cell Biol.* 2011;14(1):61-72.
30. Dowdle WE, Robinson JF, Kneist A, Sirerol-Piquer MS, Frints SG, Corbit KC, et al. Disruption of a ciliary B9 protein complex causes Meckel syndrome. *Am J Hum Genet.* 2011;89(1):94-110.
31. Roberson EC, Dowdle WE, Ozanturk A, Garcia-Gonzalo FR, Li C, Halbritter J, et al. TMEM231, mutated in orofaciodigital and Meckel syndromes, organizes the ciliary transition zone. *J Cell Biol.* 2015;209(1):129-42.
32. Chávez M, Ena S, Van Sande J, de Kerchove d'Exaerde A, Schurmans S, and Schiffmann SN. Modulation of Ciliary Phosphoinositide Content Regulates Trafficking and Sonic Hedgehog Signaling Output. *Dev Cell.* 2015;34(3):338-50.
33. Garcia-Gonzalo FR, Phua SC, Roberson EC, Garcia G, Abedin M, Schurmans S, et al. Phosphoinositides Regulate Ciliary Protein Trafficking to Modulate Hedgehog Signaling. *Dev Cell.* 2015;34(4):400-9.
34. Dyson JM, Conduit SE, Feeney SJ, Hakim S, DiTommaso T, Fulcher AJ, et al. INPP5E regulates phosphoinositide-dependent cilia transition zone function. *J Cell Biol.* 2017;216(1):247-63.
35. Ukhanov K, Uytingco C, Green W, Zhang L, Schurmans S, and Martens JR. INPP5E controls ciliary localization of phospholipids and odor response in olfactory sensory neurons. *J Cell Sci.* 2021.
36. Goetz SC, Bangs F, Barrington CL, Katsanis N, and Anderson KV. The Meckel syndrome- associated protein MKS1 functionally interacts with components of the BBSome and IFT complexes to mediate ciliary trafficking and hedgehog signaling. *PLoS One.* 2017;12(3):e0173399.
37. Uytingco CR, and Martens JR. Intranasal Delivery of Adenoviral and AAV Vectors for Transduction of the Mammalian Peripheral Olfactory System. *Methods Mol Biol.* 2019;1950:283-97.
38. McIntyre JC, Davis EE, Joiner A, Williams CL, Tsai IC, Jenkins PM, et al. Gene therapy rescues cilia defects and restores olfactory function in a mammalian ciliopathy model. *Nat Med.* 2012;18(9):1423-8.
39. Wesson DW, Varga-Wesson AG, Borkowski AH, and Wilson DA. Respiratory and sniffing behaviors throughout adulthood and aging in mice. *Behav Brain Res.* 2011;223(1):99-106.

40. Saarikangas J, Zhao H, and Lappalainen P. Regulation of the actin cytoskeleton-plasma membrane interplay by phosphoinositides. *Physiol Rev.* 2010;90(1):259-89.
41. Senju Y, Kalimeri M, Koskela EV, Somerharju P, Zhao H, Vattulainen I, et al. Mechanistic principles underlying regulation of the actin cytoskeleton by phosphoinositides. *Proc Natl Acad Sci U S A.* 2017;114(43):E8977-E86.
42. Nager AR, Goldstein JS, Herranz-Pérez V, Portran D, Ye F, Garcia-Verdugo JM, et al. An Actin Network Dispatches Ciliary GPCRs into Extracellular Vesicles to Modulate Signaling. *Cell.* 2017;168(1-2):252-63.e14.
43. Kim J, Jo H, Hong H, Kim MH, Kim JM, Lee JK, et al. Actin remodelling factors control ciliogenesis by regulating YAP/TAZ activity and vesicle trafficking. *Nat Commun.* 2015;6:6781.
44. Belin BJ, Goins LM, and Mullins RD. Comparative analysis of tools for live cell imaging of actin network architecture. *Bioarchitecture.* 2014;4(6):189-202.
45. McEwen DP, Jenkins PM, and Martens JR. Olfactory cilia: our direct neuronal connection to the external world. *Curr Top Dev Biol.* 2008;85:333-70.
46. Goldstein AL, Hannappel E, and Kleinman HK. Thymosin beta4: actin-sequestering protein moonlights to repair injured tissues. *Trends Mol Med.* 2005;11(9):421-9.
47. Garcia-Gonzalo FR, and Reiter JF. Open Sesame: How Transition Fibers and the Transition Zone Control Ciliary Composition. *Cold Spring Harb Perspect Biol.* 2017;9(2).
48. Goncalves J, and Pelletier L. The Ciliary Transition Zone: Finding the Pieces and Assembling the Gate. *Mol Cells.* 2017;40(4):243-53.
49. Jensen VL, Li C, Bowie RV, Clarke L, Mohan S, Blacque OE, et al. Formation of the transition zone by Mks5/Rpgrip1L establishes a ciliary zone of exclusion (CIZE) that compartmentalises ciliary signalling proteins and controls PIP2 ciliary abundance. *EMBO J.* 2015;34(20):2537-56.
50. Conduit SE, and Vanhaesebroeck B. Phosphoinositide lipids in primary cilia biology. *Biochem J.* 2020;477(18):3541-65.
51. Stilling S, Kalliakoudas T, Benninghoven-Frey H, Inoue T, and Falkenburger BH. PIP2 determines length and stability of primary cilia by balancing membrane turnovers. *Commun Biol.* 2022;5(1):93.
52. Malek M, Kielkowska A, Chessa T, Anderson KE, Barneda D, Pir P, et al. PTEN Regulates PI(3,4)P2 Signaling Downstream of Class I PI3K. *Mol Cell.* 2017;68(3):566-80 e10.
53. Shnitsar I, Bashkurov M, Masson GR, Ogunjimi AA, Mosessian S, Cabeza EA, et al. PTEN regulates cilia through Dishevelled. *Nat Commun.* 2015;6:8388.
54. Kim J, Lee JE, Heynen-Genel S, Suyama E, Ono K, Lee K, et al. Functional genomic screen for modulators of ciliogenesis and cilium length. *Nature.* 2010;464(7291):1048-51.
55. Janmey PA, Bucki R, and Radhakrishnan R. Regulation of actin assembly by PI(4,5)P2 and other inositol phospholipids: An update on possible mechanisms. *Biochem Biophys Res Commun.* 2018;506(2):307-14.
56. Drummond ML, Li M, Tarapore E, Nguyen TTL, Barouni BJ, Cruz S, et al. Actin polymerization controls cilia-mediated signaling. *J Cell Biol.* 2018;217(9):3255-66.
57. Zhang C, Zhang W, Lu Y, Yan X, Yan X, Zhu X, et al. NudC regulates actin dynamics and ciliogenesis by stabilizing cofilin 1. *Cell Res.* 2016;26(2):239-53.
58. Forsythe E, and Beales PL. Bardet-Biedl syndrome. *Eur J Hum Genet.* 2013;21(1):8-13.
59. Berbari NF, Lewis JS, Bishop GA, Askwith CC, and Mykytyn K. Bardet-Biedl syndrome proteins are required for the localization of G protein-coupled receptors to primary cilia. *Proc Natl Acad Sci U S A.* 2008;105(11):4242-6.
60. Shah AS, Farmen SL, Moninger TO, Businga TR, Andrews MP, Bugge K, et al. Loss of Bardet-Biedl syndrome proteins alters the morphology and function of motile cilia in airway epithelia. *Proc Natl Acad Sci U S A.* 2008;105(9):3380-5.

61. Mokrzan EM, Lewis JS, and Mykytyn K. Differences in renal tubule primary cilia length in a mouse model of Bardet-Biedl syndrome. *Nephron Exp Nephrol.* 2007;106(3):e88-96.
62. Lechtreck KF, Brown JM, Sampaio JL, Craft JM, Shevchenko A, Evans JE, et al. Cycling of the signaling protein phospholipase D through cilia requires the BBSome only for the export phase. *J Cell Biol.* 2013;201(2):249-61.
63. Liu YX, Xue B, Sun WY, Wingfield JL, Sun J, Wu M, et al. Bardet-Biedl syndrome 3 protein promotes ciliary exit of the signaling protein phospholipase D via the BBSome. *Elife.* 2021;10.
64. Leitch CC, Zaghloul NA, Davis EE, Stoetzel C, Diaz-Font A, Rix S, et al. Hypomorphic mutations in syndromic encephalocele genes are associated with Bardet-Biedl syndrome. *Nat Genet.* 2008;40(4):443-8.
65. Yee LE, Garcia-Gonzalo FR, Bowie RV, Li C, Kennedy JK, Ashrafi K, et al. Conserved Genetic Interactions between Ciliopathy Complexes Cooperatively Support Ciliogenesis and Ciliary Signaling. *PLoS Genet.* 2015;11(11):e1005627.
66. Ning K, Song E, Sendayen BE, Prosseda PP, Chang KC, Ghaffarieh A, et al. Defective INPP5E distribution in NPHP1-related Senior-Loken syndrome. *Mol Genet Genomic Med.* 2020:e1566.
67. Colin A, Singaravelu P, Thery M, Blanchoin L, and Gueroui Z. Actin-Network Architecture Regulates Microtubule Dynamics. *Curr Biol.* 2018;28(16):2647-56 e4.
68. Rouven Bruckner B, Pietuch A, Nehls S, Rother J, and Janshoff A. Ezrin is a Major Regulator of Membrane Tension in Epithelial Cells. *Sci Rep.* 2015;5:14700.
69. Braunger JA, Bruckner BR, Nehls S, Pietuch A, Gerke V, Mey I, et al. Phosphatidylinositol 4,5-bisphosphate alters the number of attachment sites between ezrin and actin filaments: a colloidal probe study. *J Biol Chem.* 2014;289(14):9833-43.
70. Pietuch A, Bruckner BR, and Janshoff A. Membrane tension homeostasis of epithelial cells through surface area regulation in response to osmotic stress. *Biochim Biophys Acta.* 2013;1833(3):712-22.
71. Wesson DW, Donahou TN, Johnson MO, and Wachowiak M. Sniffing behavior of mice during performance in odor-guided tasks. *Chem Senses.* 2008;33(7):581-96.

Figures.

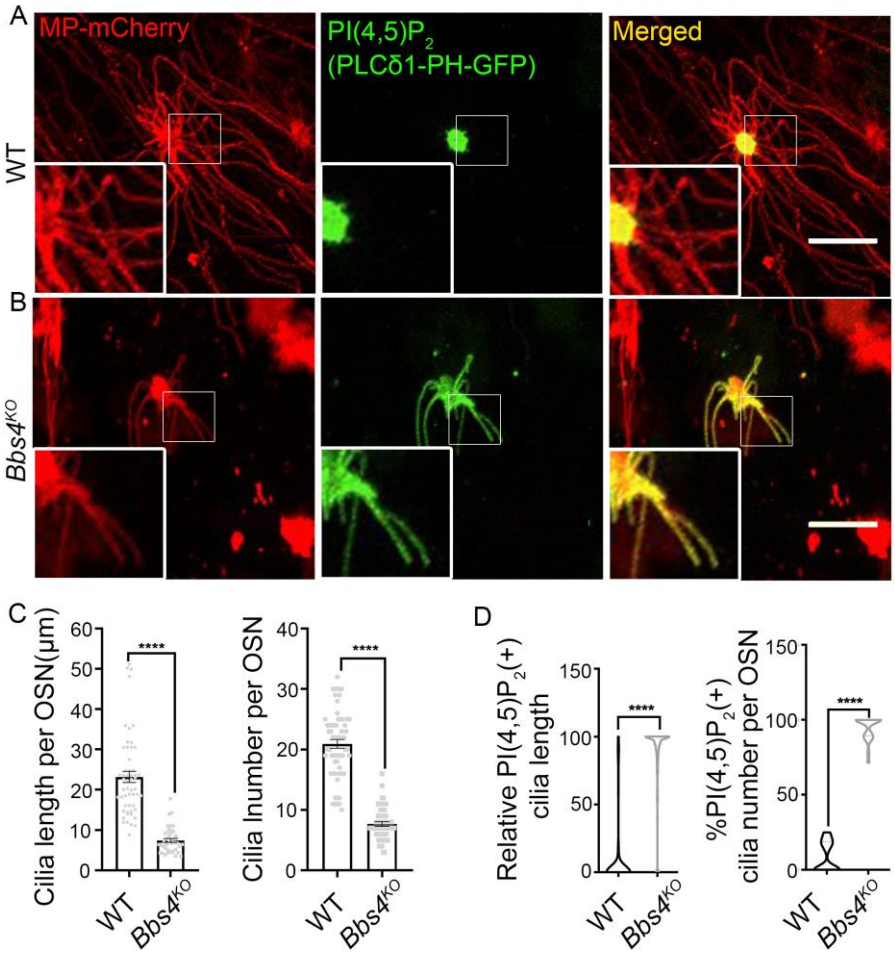

Figure 1. PI(4,5)P_2 aberrantly redistributes into olfactory cilia in *Bbs4^{KO}*. Representative *en face* images of PI(4,5)P_2 (PLCδ1-PH-GFP) in the WT **(A)** and the *Bbs4^{KO}* **(B)** olfactory cilia. 10 days post MP-mCherry and PLCδ1-PH-GFP adenovirus infection, the WT and *Bbs4^{KO}* mice were used for *en face* imaging. The endogenous PI(4,5)P_2 distribution was labeled by PLCδ1-PH-GFP and the full length of olfactory cilia was marked by MP-mCherry. Scale 10 μm. **(C)** Quantification of olfactory cilia length per OSN (left) and the cilia number per OSN (right) showing *Bbs4^{KO}* OSNs have significantly shorter (WT n=54 OSNs: 23.18± 1.382μm vs *Bbs4^{KO}* n=43 OSNs: 7.411± 0.4752 μm) and fewer olfactory cilia (WT n=61 OSNs: 20.92 ± 0.7240 vs *Bbs4^{KO}* n=51 OSNs: 7.667 ± 0.3816) compared with WT. **(D)** Quantification of relative PI(4,5)P_2 positive OSN cilia length (left) and the percentage of PI(4,5)P_2 positive cilia per OSN (right) showing *Bbs4^{KO}* OSNs have relatively longer (WT n=161 cilia: 8.347 ±1.950 vs *Bbs4^{KO}* n=124 cilia : 88.98 ±2.078） and more PI(4,5)P_2 (WT n=23 OSNs: 8.399 ±2.102 vs *Bbs4^{KO}* n=24 OSNs: 94.63 ±1.649) redistributed cilia. Unpaired t-test, **** p<0.0001. Values represent means ± SEM.

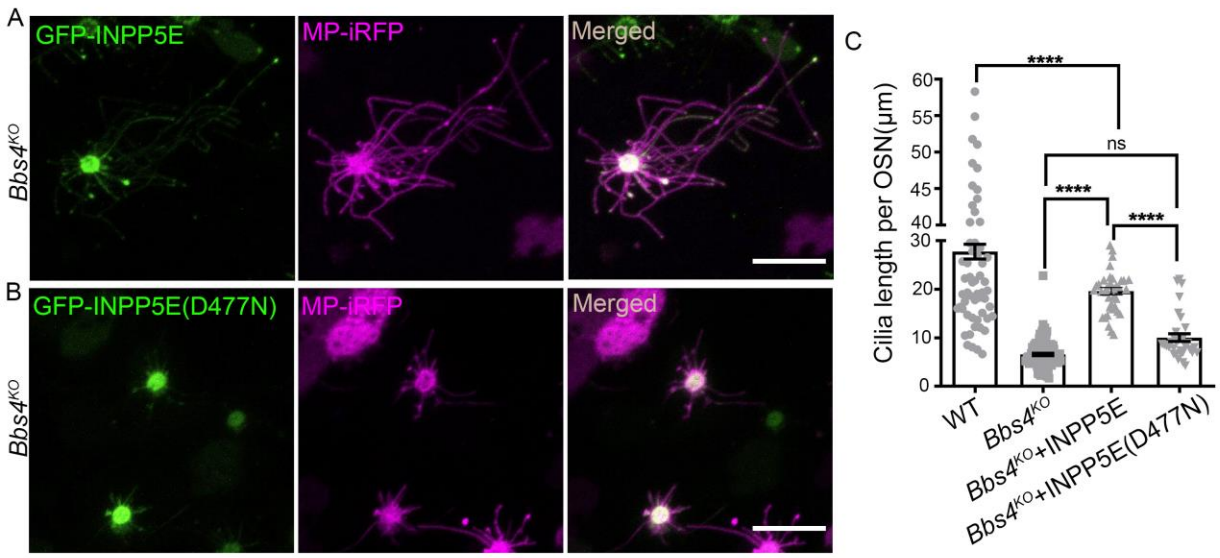

Figure 2. Ectopic expression of INPP5E rescues olfactory cilia length in *Bbs4^{KO}*. Representative *en face* images of adenoviral expressed GFP-INPP5E **(A)**, or GFP-INPP5E(D477N) **(B)** and MP-iRFP in olfactory cilia of *Bbs4^{KO}*. Scale 10 µm. **(C)** Quantification of olfactory cilia length per OSN showing a significant increase in cilia length of *Bbs4^{KO}* OSNs with INPP5E infection (WT: n=76 OSNs: 27.74 ± 1.513; *Bbs4^{KO}*: n=115 OSNs: 6.593 ± 0.2584; *Bbs4^{KO}*+INPP5E: n= 38 OSNs: 19.61± 0.7611; *Bbs4^{KO}*+ INPP5E(D477N): n= 34 OSNs: 10.06± 0.7922). One-way ANOVA, ****p < 0.0001, Values represent means ± SEM.

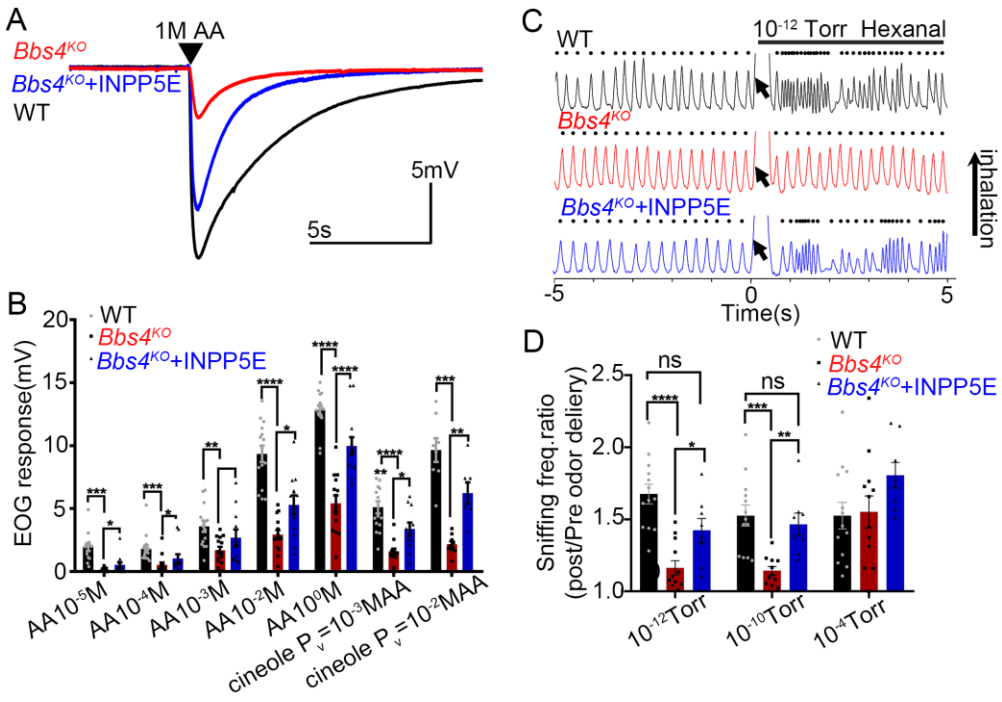

725

726 **Figure 3. Overexpression of INPP5E rescues the impaired peripheral odor detection and odor**
727 **perception of *Bbs4*^{KO} mice. (A)** Representative electro-olfactogram (EOG) recordings traces from the
728 surface of the olfactory epithelium (OE) of WT, *Bbs4*^{KO} and INPP5E treated *Bbs4*^{KO} (*Bbs4*^{KO}+INPP5E) mice
729 in response to the delivery of 10^0 M of amyl acetate (AA). Arrowhead indicates the time point of odor delivery.
730 **(B)** Quantified EOG data showing the reduced peripheral odor detection to different concentration amyl
731 acetate (AA), and cineole in *Bbs4*^{KO} mice had been significantly restored by ectopic expression of INPP5E.
732 $P_{V:}$ vapor pressure. (WT: n=12 animals; *Bbs4*^{KO}: n=10 animals; *Bbs4*^{KO}+INPP5E: n=10 animals). **(C)**
733 Representative plethysmograph traces prior to and during delivery of 10^{-12} Torr hexanal (arrow). Odorant
734 (arrow) failed to elicit high frequency sniffing in *Bbs4*^{KO} mouse (middle) which were readily apparent in the
735 WT (top) and INPP5E treated *Bbs4*^{KO} (*Bbs4*^{KO}+INPP5E) (bottom). **(D)** Detection thresholds of 13 WT, 12
736 *Bbs4*^{KO}, and 8 *Bbs4*^{KO} +INPP5E mice (average of 4 odors / mouse) indicating that reduced odorant
737 sensitivity (increased detection thresholds) in *Bbs4*^{KO} mice can be reduced by INPP5E treatment. The
738 mouse was delivered 10 trials of vaporized mineral oil followed by presentations of an odorant at 10^{-12}, 10^{-10}, and 10^{-4}Torr. Sniffing frequency ratios (sniffing Hz pre vs during odor) were compared between groups.
740 One way ANOVA, ****p < 0.0001. ***p < 0.001. **p < 0.01.*p < 0.05. Values represent means ± SEM.

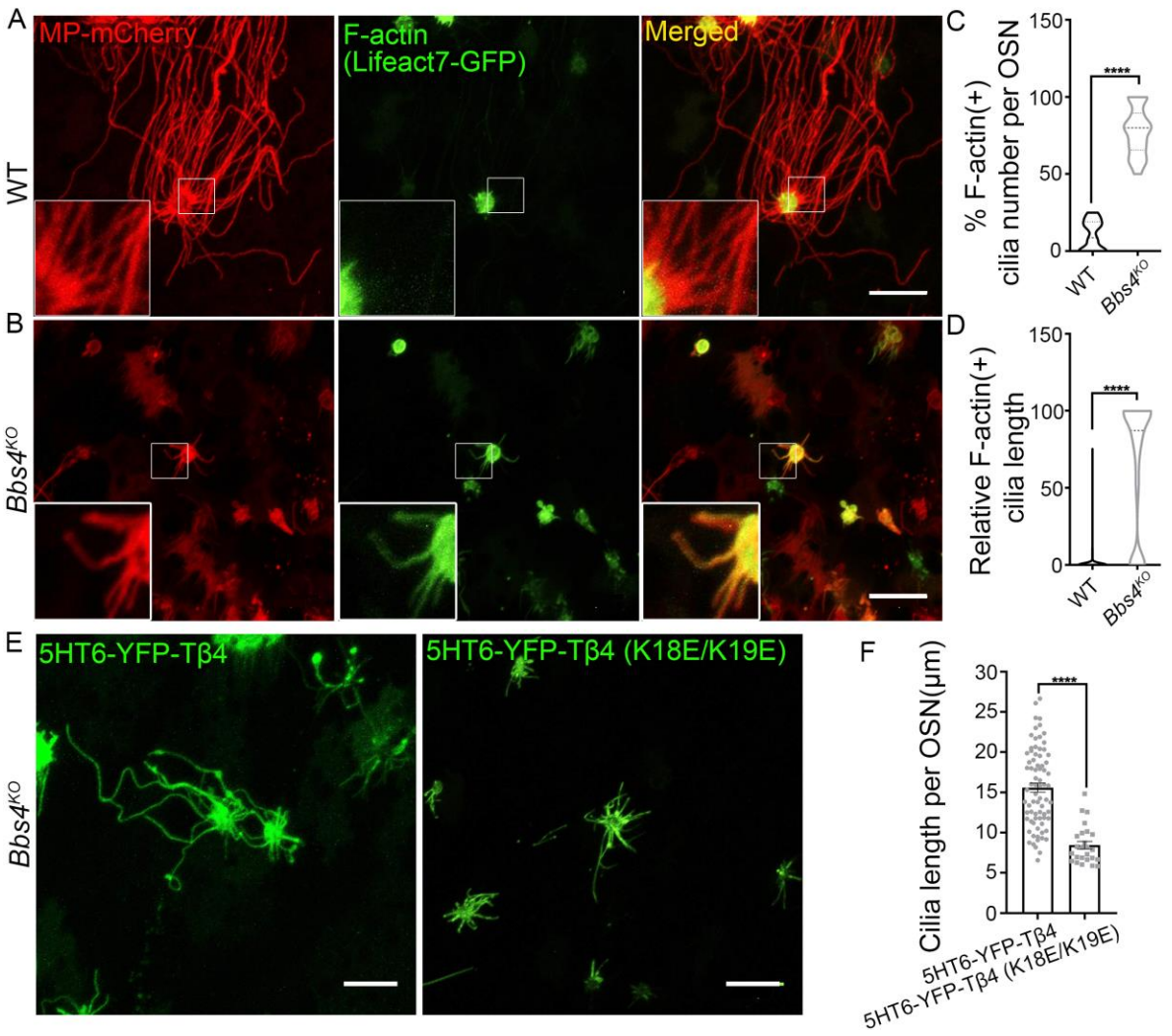

741

742 **Figure 4. F-actin infiltrates into olfactory cilia in *Bbs4*^{KO}, which is necessary for *Bbs4*^{KO} olfactory cilia**
743 **shortening.** Representative *en face* images of F-actin (Lifeact7-GFP) ciliary distribution in the WT **(A)** and
744 *Bbs4*^{KO} **(B)** OSNs. The WT and *Bbs4*^{KO} mice were co-infected with MP-mCherry and Lifeact7-GFP adenovirus
745 and used for *en face* imaging 10 days post virus infection. MP-mCherry was used to label the full length of the
746 olfactory cilia. Lifeact7-GFP was used to label the endogenous F-actin. **(A)** F-actin was excluded from the
747 olfactory cilia in the WT group. **(B)** F-actin lost its restriction in the knob of OSN and redistributed in the
748 olfactory cilia in *Bbs4*^{KO}. Scale 10 μm. **(C)** Quantification data showing that the percentage of F-actin positive
749 cilia number (F-actin positive cilia number/total cilia number*100) was significantly increased in the *Bbs4*^{KO}
750 group (n=38 OSNs, 77.32±2.494) compared to the WT group (n=34 OSNs, 10.37±1.615). Unpaired t-test,
751 ****p<0.0001. **(D)** The relative F-actin positive cilia length (F-actin positive cilia length/ full cilia length*100) was
752 significantly increased in *Bbs4*^{KO} (n=272 cilia from 38 OSNs, 66.31± 2.531) compared to the WT group (n=597
753 cilia from 34 OSNs, 1.751± 0.3133). Unpaired t-test, ****p<0.0001. **(E)** Representative *en face* images of the
754 5HT6-YFP-Tβ4 (left) and 5HT6-YFP-Tβ4 (K18E/K19E) (actin-binding mutant) (right) treated *Bbs4*^{KO} olfactory
755 cilia. Scale 10 μm. **(F)** Quantification of olfactory cilia length showed that *Bbs4*^{KO} olfactory cilia length was
756 partially rescued by 5HT6-YFP-Tβ4 treatment (5HT6-YFP-Tβ4: n=51 OSNs: 15.60 ± 0.5596 vs 5HT6-YFP-
757 Tβ4 (K18E/K19E): n=25 OSNs: 8.448 ± 0.4769). Unpaired t-test, **** p<0.0001. Values represent means ±
758 SEM.

759

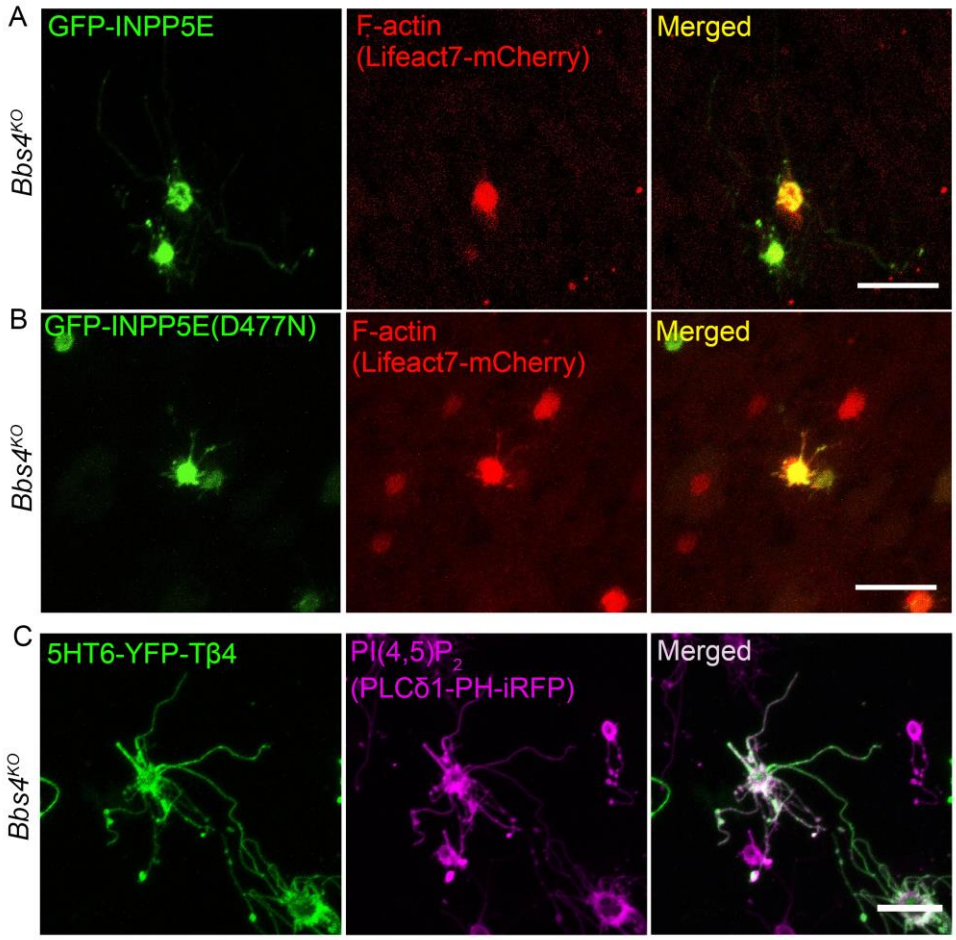

760

761 **Figure 5. PI(4,5)P_2 directly controls F-actin ciliary distribution in *Bbs4^{KO}* OSNs. (A)** Representative *en*
762 *face* images of F-actin (Lifeact7-mCherry) ciliary distribution in GFP-INPP5E infected *Bbs4^{KO}* OSN. The
763 expression of GFP-INPP5E blocked F-actin ciliary abnormal localization in *Bbs4^{KO}*. **(B)** Representative *en*
764 *face* images of F-actin (Lifeact7-mCherry) ciliary distribution in GFP-INPP5E(D477N) treated *Bbs4^{KO}* OSN.
765 F-actin infiltrated into the olfactory cilia after treatment GFP-INPP5E(D477N). **(C)** *En face* images of
766 PI(4,5)P_2 (PLCδ1-PH-iRFP) ciliary redistribution in 5HT6-YFP-Tβ4 expressed *Bbs4^{KO}* OSN. PI(4,5)P_2 still
767 redistributed into the olfactory cilia in 5HT6-YFP-Tβ4 treated *Bbs4^{KO}* OSN. Scale 10 μm.

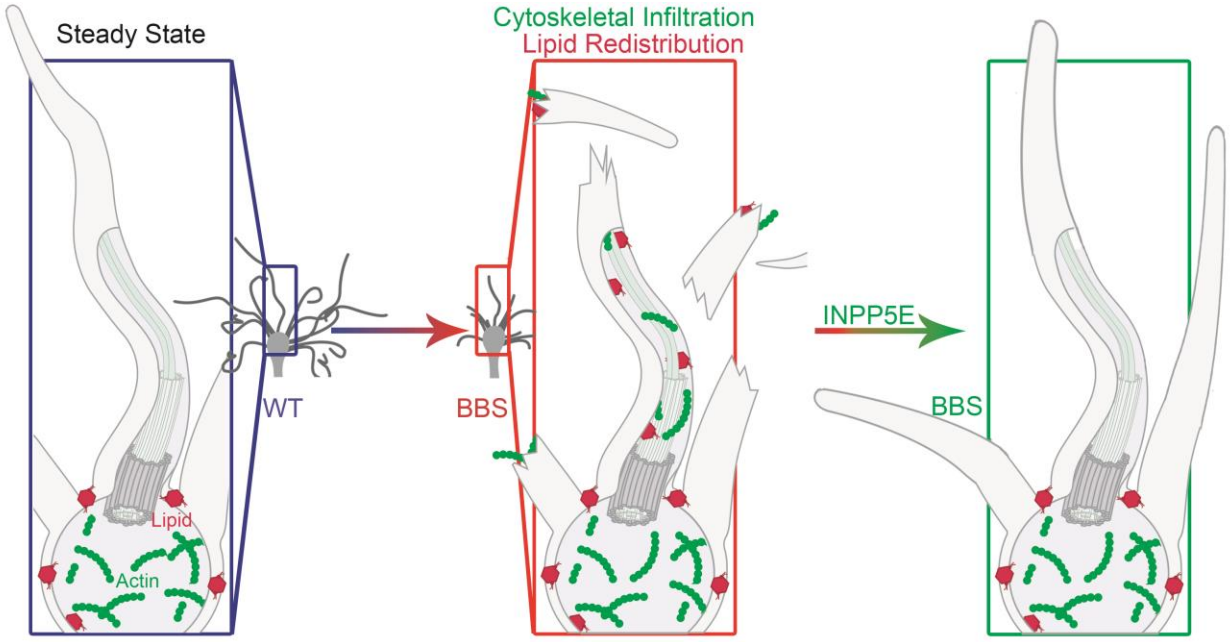

Figure 6. Schematic representation of the underlying mechanisms of olfactory cilia shortening in BBS. The distribution of $PI(4,5)P_2$ and F-actin are normally restricted to the knob of the WT OSN. However, in olfactory cilia in BBS, the dysfunctions in BBSome lead to aberrantly $PI(4,5)P_2$ ciliary redistribution and F-actin infiltration, which are necessary for olfactory cilia shortening and contribute to the pathogenesis of BBS. Blocking $PI(4,5)P_2$ and F-actin ciliary mislocalization by adenoviral expression of INPP5E restores olfactory cilia length in BBS, which therefore rescues defects in peripheral odor detection and odor perception of BBS.